

Hydrogen adsorption in metal-organic frameworks: the role of nuclear quantum effects

Mohammad Wahiduzzaman,¹ Christian F. J. Walther,¹ and Thomas Heine^{1, a)}
School of Engineering and Science, Jacobs University Bremen, D-28759 Bremen, Germany

(Dated: August 3, 2021)

The role of nuclear quantum effects on the adsorption of molecular hydrogen in metal-organic frameworks (MOFs) has been investigated on grounds of Grand-Canonical Quantized Liquid Density-Functional Theory (GC-QLDFT) calculations. For this purpose, we have carefully validated classical H₂-host interaction potentials that are obtained by fitting Born-Oppenheimer ab initio reference data. The hydrogen adsorption has first been assessed classically using Liquid Density-Functional Theory (LDFT) and the Grand-Canonical Monte Carlo (GCMC) methods. The results have been compared against the semi-classical treatment of quantum effects by applying the Feynman-Hibbs correction to the Born-Oppenheimer-derived potentials, and by explicit treatment within the Grand-Canonical Quantized Liquid Density-Functional Theory (GC-QLDFT).

The results are compared with experimental data and indicate pronounced quantum and possibly many-particle effects. After validation calculations have been carried out for IRMOF-1 (MOF-5), GC-QLDFT is applied to study the adsorption of H₂ in a series of MOFs, including IRMOF-4, -6, -8, -9, -10, -12, -14, -16, -18 and MOF-177. Finally, we discuss the evolution of the H₂ quantum fluid with increasing pressure and lowering temperature.

PACS numbers: 02.70.Uu, 05.30.-d, 05.30.Jp, 05.70.Ce, 64.30.Jk, 68.43.-h, 88.30.-k, 88.30.R-

Keywords: QLDFT, GCMC, MOFs, H₂ adsorption, quantum effects

I. INTRODUCTION

A CO₂ neutral economy requires efficient technologies for the storage and transport of energy carriers. Chemical storage is the most likely solution of this problem, as we know no other carrier that can reversibly store and release energy in similar quantity. Molecular hydrogen (H₂) is the chemical system with the highest energy per mass unit. Moreover, it can be produced by water splitting, and its oxidation product is environmentally benign. Hydrogen already plays an important role in the development of alternative transport systems. It is, however, limited by the difficulty to generate a hydrogen transport system that has a sufficient gravimetric and volumetric storage capacity. One of the promising hydrogen storage systems that have been discussed extensively are metal-organic frameworks (MOFs). MOFs are materials with very large internal surface area, and thus they are capable of adsorbing significant amounts of H₂ at liquid nitrogen temperature ($T = 77$ K) and moderate pressures.¹

In nanoporous materials such as MOFs, H₂ is adsorbed by physisorption, that is by weak, attractive interactions. Depending on the chemical nature of the pore surfaces we distinguish between strong adsorption sites, where a charge center at the MOF induces a dipole moment in the adsorbed H₂ molecule and attracts it by up to ~ 40 kJ mol⁻¹, and weak adsorption on the surface of the framework, with typical interaction energies in the 3-6

kJ mol⁻¹ range. The strong adsorption sites can be occupied at high temperature, while the weak ones are only attractive to hydrogen molecules at liquid nitrogen temperatures and below.² As the number of strong attraction sites is limited by the framework topology and – due to the incorporation into the framework – cover only a relatively small volume of the pores, their presence is not sufficient to allow for sizeable room temperature adsorption. For low temperatures, however, they are responsible for a relatively high local density of the liquid hydrogen fluid, but the main amount of adsorbed hydrogen is found to be rather homogeneously distributed over the pore surface. Thus, at low temperature the internal surface area of a MOF is the determining factor of its hydrogen storage capacity.³

A large number of MOF structures have been synthesized and studied in the last decade,⁴⁻⁷ some of them show remarkable surface areas and hydrogen storage capacities.^{1,8,9} One of the most notable examples is MOF-210 with 6240 m² g⁻¹ BET surface area, which can adsorb 176 mg g⁻¹ H₂ at 77 K.⁶ In this work we explore the nature of the adsorbed hydrogen fluid by calculations that consider explicitly its quantum mechanical nature. In order to achieve this goal, we have carefully validated our computational approach. First, available force fields (FF) to describe the interaction between H₂ and the MOF framework have been compared. Based on extensive validation calculations, we have selected the FF of Fu et al.,¹⁰ a force-field that has been parametrized from ab initio calculations and that resembles the Born-Oppenheimer (BO), that is classical interaction between hydrogen and the framework. Quantum effects can then be included either by semi-classical correction (Feynman-

^{a)}To whom correspondence should be addressed. Electronic mail: t.heine@jacobs-university.de

Hibbs (FH)),¹¹ or directly included into the Hamiltonian as kinetic energy operator.^{12–14} We further benchmark our approach and assess the different approximations by their influence on the adsorption properties of the H₂ quantum fluid. Finally, after careful validation on MOF-5, we apply our method, the Grand-Canonical Quantized Liquid Density-Functional Theory (GC-QLDFT) to a series of MOFs.

II. QUANTIZED LIQUID DENSITY-FUNCTIONAL THEORY

Realistic theoretical simulations of H₂ adsorption at high densities are essential in guiding the design of hydrogen adsorbent materials. In principle, a wide range of statistical mechanics based simulation techniques is available for this purpose, including Grand Canonical Monte Carlo (GCMC),¹⁵ molecular dynamics (MD), and classical Density-Functional Theory of Liquids (LDFT).¹⁶ In most cases, quantization of nuclear motion of the hydrogen guest molecules is not explicitly considered in the simulations. Although quantum effects can be treated rigorously with path-integral (PI) techniques, e.g. in PI-GCMC,¹⁷ such simulations are quite elaborate and are not always trivial to interpret. Instead, it is common to semi-classically include quantum effects in the interaction potential, either by using the Feynman-Hibbs correction,¹¹ or by using force fields that have been optimized to match experimental results.¹⁸

In 2009, Patchkovskii and Heine suggested to include quantum effects into LDFT. In the Quantized LDFT (QLDFT), they employed the Kohn-Sham technique to introduce an effective non-interacting system of one-particle wave functions, for which the kinetic energy operator is explicitly known.¹² For liquid nitrogen temperatures (77 K) and above, the particles can be described equally well using a Stefan-Boltzmann or Bose-Einstein statistics.¹⁹ Many-particle effects are implicitly included in the excess, or exchange-correlation functional (XC).^{12,13} As common in electronic DFT, the XC functional also accounts for any further approximations and models, and two XC approximations have been suggested: the local density approximation (LDA), and the non-local weighted density approximation (WDA). By construction, QLDFT is exact for the uniform hydrogen gas. The implementation of QLDFT takes advantage of the sparsity of the Hamiltonian at higher temperature.²⁰ For lower temperatures, the sparsity is strongly reduced, resulting in an increase of memory and computational requirements. In these cases, QLDFT is not computationally competitive, and consequently only few applications have been reported so far. The QLDFT method has been successfully applied in the hydrogen adsorption studies in carbon foams,¹³ porous aromatic frameworks (PAFs)²¹ and to determine the selectivity of D₂ vs. H₂ adsorption in the metal-organic framework MFU-4.²²

A low-temperature alternative to the Kohn-Sham

scheme of QLDFT has been suggested recently¹⁴: due to the bosonic nature of molecular hydrogen, at low temperatures the lowest eigenstate dominates the occupation of the Kohn-Sham Hamiltonian. Thus, the quantum-mechanical problem was reformulated within the Hohenberg-Kohn-Mermin formalism of a Grand Canonical (GC) ensemble.

In GC-QLDFT, we directly minimize the density. However, we introduce a pseudo-wavefunction that satisfies the equation $\rho(\vec{r}) = \psi^2(\vec{r})$. The main purpose of this wave function is to be able to approximate the kinetic energy operator, which we can now conveniently write within the effective one particle approximation¹⁴:

$$T[\rho] = -\frac{\hbar^2}{2m} \int d^3r \tilde{\psi} \nabla^2 \tilde{\psi}. \quad (1)$$

The GC-QLDFT free energy functional is then given by:

$$F[\rho] = -\frac{\hbar^2}{2m} \int d^3r \tilde{\psi} \nabla^2 \tilde{\psi} + F_H[\rho] + F_{xc}[\rho] + \int d^3r v_{\text{ext}}(\vec{r})\rho(\vec{r}), \quad (2)$$

where F_H is the Hartree term, F_{xc} the excess correction and v_{ext} denotes the external potential.

Quantum effects are thus included explicitly in the kinetic energy term which is responsible that the density vanishes correctly close to regions with a huge external potential. Quantum effects are also included approximately in F_{xc} , which is constructed to match the experimental data.¹⁴

It is worth noting that it is difficult to compare classical and quantized LDFT, as the QLDFT functional was constructed to fulfil the uniform fluid limit exactly, realized by including the experimental free energy explicitly in F_{xc} , while the classical theory starts from the Helmholtz free energy of the ideal gas and includes additional corrections. Both methods typically include the weighted density $\bar{\rho}$ in the excess functional.

As in other DFT schemes, QLDFT strongly benefits from removal of systematic errors which is achieved by requesting that experimental reference data such as the uniform fluid limit is matched exactly. This way, various approximations that are made for the sake of numerical simplicity are compensated to a large extent. This includes the shapeless particle approximation, the one-effective-particle approximation for the kinetic energy, and even many-body effects between the particles.

The resulting grand potential is minimized by employing the Car-Parrinello technique,²³ allowing for an efficient treatment of low-temperature systems, even if the host structure requires a very large unit cell for its proper description.¹⁴ In this work, we employ this variant of QLDFT within the GC ensemble (GC-QLDFT). In order to avoid long abbreviations, we will label this method as QLDFT in the remainder of this work.

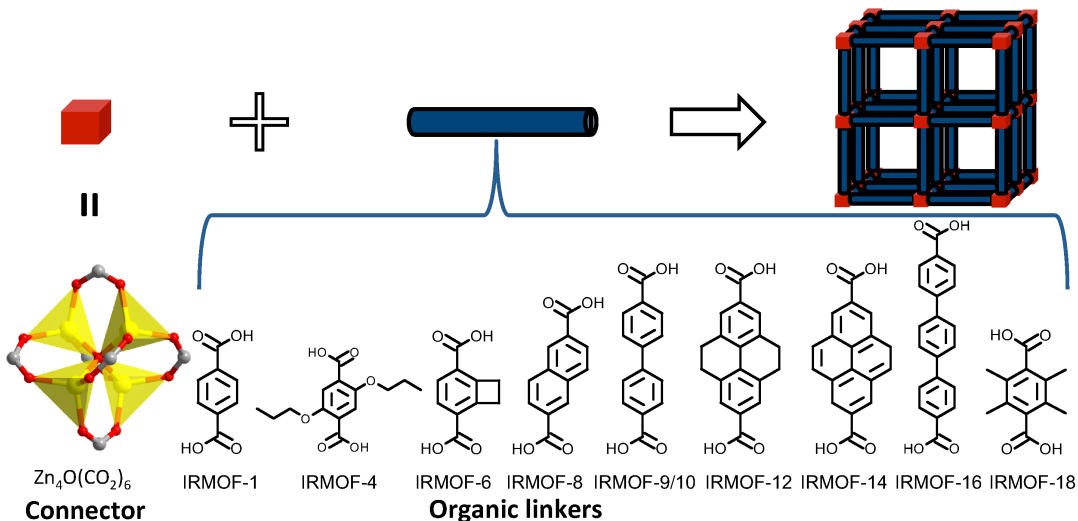


Figure 1. Schematic representation of the structure topology of $\text{Zn}_4\text{O}(\text{CO}_2)_6$ -based IRMOFs.

III. COMPUTATIONAL METHODS AND MODELS OF THE MATERIALS

GCMC simulations of hydrogen adsorption were performed with the multipurpose simulation code Music.²⁴ The sorbent model was described by a finite three-dimensional periodic $2 \times 2 \times 2$ supercell. A tail cutoff of 12.8 Å was applied to calculate pair-wise van-der-Waals interactions. Each Monte Carlo (MC) move consisted of an insertion attempt of a new molecule, the deletion or translation of an existing molecule. The probability of each of these moves were equally weighted. Since the H_2 molecules have been modeled as shapeless particles, rotation and intramolecular moves were neglected. For each point on the isotherm, three million MC steps were carried out to equilibrate the system, and a further two million MC steps were performed to calculate the ensemble average. The non-ideal behavior of adsorption isotherms at high pressure have been corrected by using the gas-phase fugacities calculated with Leachman et al.’s²⁵ equation of states (EOS). Quantum effects were included by correcting the H_2 - H_2 and H_2 -host potentials using the Feynman-Hibbs (FH)¹¹ formula:

$$V_{\text{FH}}(r) = V(r) + \frac{\hbar^2}{24\mu k_B T} \nabla^2 V(r), \quad (3)$$

where $V(r)$ is the classical potential energy function, μ is the reduced mass of interacting particles, and k_B is the Boltzmann constant.

The QLDFT calculations have been carried out within the qLIE1 approximation, thus including many-body interparticle interactions and quantum effects implicitly through the excess functional.¹⁴ QLDFT calculations use a grid spacing of 0.2 Å and a potential cutoff of 5000 K. For the classical LDFT variant, the cLIE XC functional has been employed, while all other simulation parameters

are identical to QLDFT.

One of the results of our simulations is the total amount of adsorbed H_2 , that is the total number of adsorbed molecules N_{tot} present in the simulation box. In experiment, the excess amount adsorbed is measured. In order to compare our results with experiment, we define the excess adsorption as

$$N_{\text{ex}} = N_{\text{tot}} - \rho_{\text{g}}(T, P)V_{\text{free}}, \quad (4)$$

where $\rho_{\text{g}}(T, P)$ is the bulk gas density at given temperature and pressure obtained from Leachman et al.’s²⁵ EOS, and V_{free} is the H_2 accessible free volume. This latter quantity is calculated as the volume within the unit cell where the potential acting on a single H_2 molecule is less than 5000 K.

The solvent accessible surface areas (SASA) were calculated by rolling a probe molecule along the van-der-Waals spheres of the atoms of the MOF structure.²⁶ This type of surface area is resulting from the center of the probe molecule, i.e., the surface corresponds to an extended sphere of each atom with a distance equal to the atom radius plus the probe radius from the center of the atoms. A probe molecule with a diameter of 2.96 Å was used which is equal to the Lennard-Jones σ parameter of H_2 molecule and commonly used in other H_2 molecular simulations.^{27,28} We employed the VMD molecular visualization software^{29,30} for the solvent accessible surface calculation.

Isorecticular MOFs (IRMOFs) are a series of molecular frameworks having identical structural topology. The members of the IRMOF series share the same connecting SBU, but different organic linkers provide a systematic variation of pore size. The series of isorecticular MOFs studied in this work are IRMOF-n with n=1, 4, 6, 8, 9, 10, 12, 14, 16, 18 is derived from linking the octahedral zinc acetate unit $\text{Zn}_4\text{O}(\text{CO}_2)_6$, with a variety of linear ditopic carboxylates^{4,31} (see Figure 1).

MOF-177 is constructed from the same connecting SBU and the tritopic BTB linker.⁵ All the IRMOFs except IRMOF-4, are adopted from the work of Kuc et al.,³² who have optimized the structures by density-functional based tight-binding (DFTB) calculations. The IRMOF-4 structure was constructed from the reported crystal structure data.⁴ The MOF-177 crystal structure was obtained from Lukose et al.,³³ again resembling DFTB optimized structures. The structural properties of these MOFs are given in Table I.

IV. THE FREE HYDROGEN GAS

It is accepted text-book knowledge that the ideal gas approximation is sufficient to treat the free hydrogen gas. Indeed, this statement is true for a wide range of temperatures and pressures. In Figure 2, various hydrogen reference isotherms at a temperature of 75 K are shown and compared with the experimental data obtained by Goodwin et al.³⁴ Surprisingly, up to a pressure of 100 bar, the ideal gas isotherm is closer to experiment than the van-der-Waals isotherm obtained from parameters as published by the National Institute of Standards (NIST),³⁵ which underestimates hydrogen densities starting from pressures of 70 bar. At a pressure of 200 bar, those two isotherm approximations are unsuitable, as the ideal gas equation overestimates the hydrogen density by 30%, while the real gas isotherm underestimates it by $\sim 20\%$. For lower temperatures, those differences are expected to get even worse.

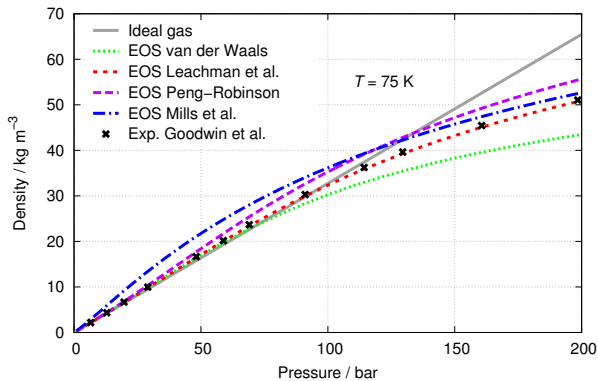


Figure 2. Bulk H_2 densities at $T = 75$ K calculated from different EOS^{25,36–38} are compared with experimental data of Goodwin et al.³⁴ The grey line represents the ideal gas.

Motivated by this deficiency of simple model isotherms, various groups have parametrized hydrogen isotherms from experimental data. We have compared data obtained from parametrized EOS by Mills et al.,³⁸ Peng and Robinson³⁷ and Leachman et al.²⁵ The former two parametrizations overestimate the hydrogen density at 75 K in the entire range of pressures. In particular, the isotherm of Mills et al. performs rather poorly at pres-

ures around 50 bar. At high pressure, however, they agree much better with the experimental data than the ideal or van-der-Waals gas isotherms. Excellent agreement with experiment is achieved by the EOS proposed by Leachman and coworkers.²⁵ At 75 K, the resulting isotherm matches the experiments of Goodwin et al.³⁴ perfectly. Therefore, we have implemented this EOS into our QLDFT code and use it for this and forthcoming studies that aim at temperatures around 77 K. At this point, it is important to note that at lower temperatures, ortho- and para-hydrogen behave differently, thus the performance of the EOS should be reassessed for the particular application that is examined. We further want to stress that even at low pressure applications, the internal pressure at strong adsorption sites is typically much higher than the external pressure. Thus, the EOS must be valid for a wide range of pressures if hydrogen adsorption problems are to be studied.

State-of-the-art atomistic methods to treat gas adsorption (GCMC, QLDFT) consider the situation that a significant part of the problem is the treatment of the interactions between the adsorbed guest molecules. Indeed, the accurate treatment of the interaction between hydrogen molecules is quite involved. In fact, H_2 molecules are finite-size particles with a directional quadrupole moment, and many-particle contributions do exist.¹³ In this work, H_2 molecules are modeled as single shapeless particles (that is, points) that are subject of pairwise interactions. For the interaction between these particles, we employ the classical (BO) potential of Diep and Johnson (DJ), that has been obtained on grounds of high-level ab initio theory with extrapolation to the basis set limit and correlation contributions.³⁹ The distance-dependent term is parametrized in a Lennard-Jones (LJ) potential, while the orientations of the hydrogen molecules with respect to each other is taken into account by a series expansion in spherical harmonics. We employ only the leading term of the DJ series, what is consistent with the shapeless particle approximation of the H_2 molecule. It is important to note that this potential reflects the BO potential and hence does not include nuclear quantum effects, making it particularly suitable for using it within QLDFT.

A semi-classical alternative to the BO potential has been suggested by Michels et al.,⁴⁰ who adjusted LJ parameters to match the second virial coefficient, thus reflecting experimental PVT data of a temperature range of 98–423 K. We have compared both of the H_2 - H_2 interaction potentials in Figure 3. Michels et al.’s data is close to the DJ potential at repulsion-dominated ranges, while the long-range interactions are closer to the FH-corrected DJ curve.

We have applied GCMC simulations to describe the free hydrogen gas, studied at 77 K and in the pressure range of 0–100 bar. In Figure 4, these calculations are benchmarked against our reference EOS by Leachman et al.²⁵ For the classical treatment (GCMC with BO DJ potential), the hydrogen density is strongly overestimated.

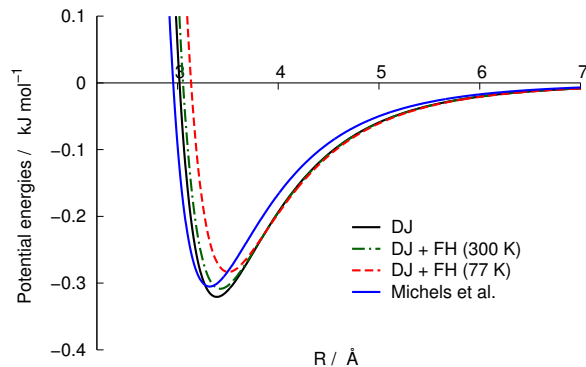


Figure 3. Comparison of classical and Feynman-Hibbs quantum corrected potentials of H_2 - H_2 interactions as function of the distance (R) between the centers of mass of the H_2 molecules.

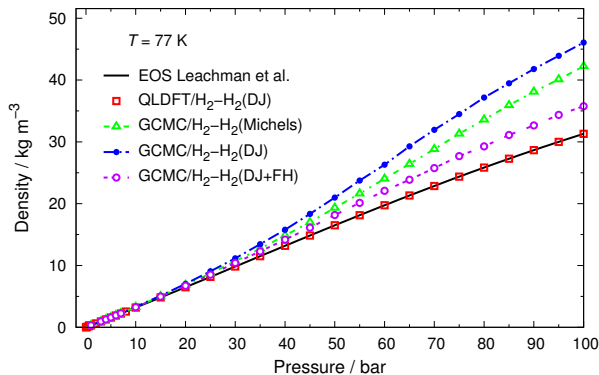


Figure 4. Real gas densities obtained from QLDFT and GCMC are compared with the EOS of Leachman et al.²⁵

Already at pressures of 30 bar, it expects a 14% higher hydrogen density, and at 100 bar, the overestimation is 47%. The situation improves for the semi-classical quantum treatment, where the best performance is obtained for the FH-corrected DJ potential. Still, a GCMC calculation employing the FH-corrected DJ potential overestimates the H_2 density by 14% at 100 bar. On the other hand, by construction QLDFT results match Leachman et al.’s isotherm perfectly. We conclude that treatment of the free hydrogen gas using pairwise semi-classical potentials results in a significant overestimation of the hydrogen density at higher pressures.

V. HOST-GUEST INTERACTION POTENTIALS

The host material acts via the external potential on the adsorbed molecules. Thus, the external potential determines the adsorption properties of the metal-organic framework. The repulsive part of the external potential defines the inaccessible volume inside the framework and thus its inner surface. The surface is rather sharply de-

fined as the potential energy curve is very steep at this region. The attractive part acts on the adsorbed gas like a local pressure enhancement and thus increases the hydrogen density at the surface. For a correct description of the adsorbed H_2 fluid the quality of the interaction potential is crucial. However, due to fortuitous error compensations, calculated thermodynamic properties may be close to experiment also for rather inaccurate external potentials.

The interaction of H_2 with the MOF framework is governed by London dispersion interactions (LDI) that are known to be difficult to be described at the quantum-mechanical level and at low computational cost. The state-of-the-art is to employ classical two-body force field with an attractive r^{-6} component for the long-range contribution, and the repulsive part either described as repulsive r^{-12} (Lennard-Jones) or by an exponential (Buckingham) term. If the adsorption calculation includes quantum effects as in QLDFT or PI-GCMC, then the external potential must be strictly classical, that is, it needs to resemble the BO surface. If, on the contrary, a classical adsorption calculation is pursued, as in GCMC, LDFT or MD, then quantum effects could be treated semi-classically, either by adding the Feynman-Hibbs correction to the potential, or by parametrizing the FF such that experimental data are matched in the validation calculations. Here, we will only consider FFs that are designed to predict the BO surface of MOFs, thus eliminating empirical influences as much as possible.

In Figure 5, we compare various interaction potentials of H_2 with atom types that are relevant for MOFs. Already at the first glance it is evident that these potentials are significantly different. They disagree with the intercept with the energy axis – that is the position that roughly defines the internal surface, and with the magnitude of the attraction of the respective atomic center with adsorbed H_2 . It is indeed surprising that many of them have been applied to MOFs, often with comparable conclusions. As aromatic carbon atoms provide a significant part of the LDI in MOFs, we will discuss here the H_2 -C potential in more detail. The only parameters that have explicitly been developed for MOFs are those of Fu et al.¹⁰ and Han et al.⁴⁴ Those are less attractive compared to parameters that have been developed for all-carbon systems, e.g. those of Patchkovskii et al.⁴⁶ and of Heine et al.⁴⁵ Cao et al.’s⁴³ parameters have been optimized for covalent-organic frameworks on the basis of MP2 calculations and also belong to the group of strongly attractive FFs. On the other hand, the generic FFs (UFF,⁴² DREIDING,⁴¹ and DREIDING with replaced H-H interactions following Michel’s pure gas isotherm⁴⁰) are less attractive, which is expected as they should include quantum effects. In the FF of Han et al.⁴⁴ it is evident that no attraction is seen in the H_2 -H potential, which is compensated by the stronger attractive H_2 -C interaction. A similar effect is present in the H_2 -Zn and H_2 -O interactions, where Han et al.’s FF is strongly attractive to Zn, but less attractive to O in comparison to Fu et al.’s¹⁰

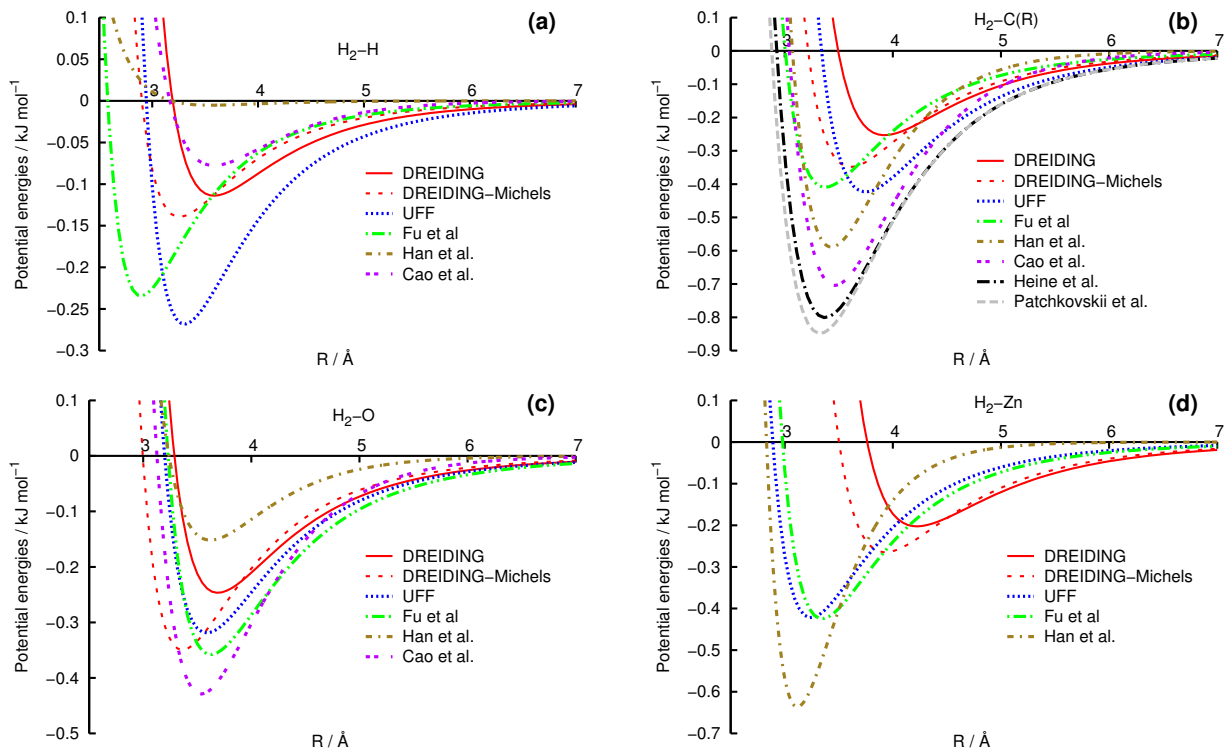


Figure 5. Typical interaction potentials between a hydrogen molecule and framework atoms: H (a), C (b), O (c) and Zn (d) in the commonly used DREIDING⁴¹ and UFF⁴² force fields, compared with ab initio parameterized force fields by Cao et al.,⁴³ Han et al.,⁴⁴ Fu et al.,¹⁰ Heine et al.⁴⁵ and Patchkovskii et al.⁴⁶ R is the distance between the center of mass of the H₂ and the framework atom

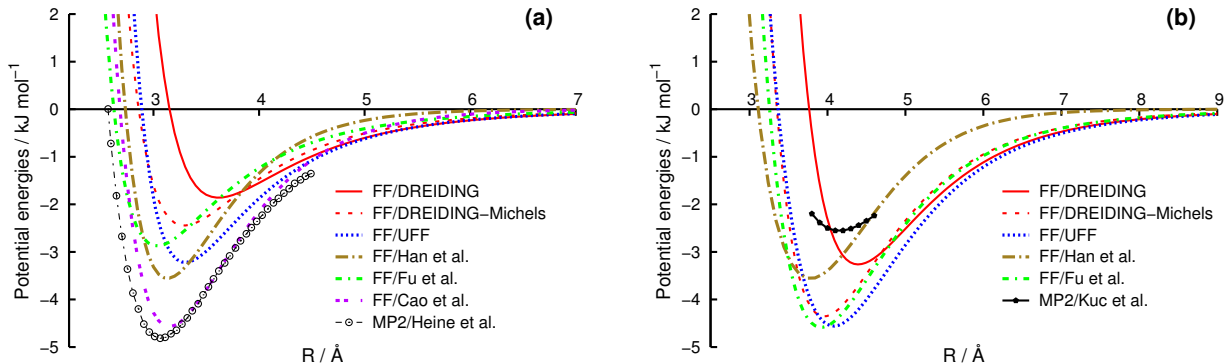


Figure 6. Potential energy curves of H₂ interacting with Benzene and Zn₄O(HCO₂)₆ molecules, determined by different force fields, are compared with MP2 results: (a) a spherical H₂ molecule moved along a line perpendicular to the benzene plane and (b) a spherical H₂ molecule moved along the Zn-O axis in the α site of the Zn₄O(HCO₂)₆ cluster. MP2 data points of Heine et al.⁴⁵ and Kuc et al.⁴⁷ are for diatomic H₂ molecules, where H₂ molecules are oriented parallel to the axis of translation. R is the distance between the centers of mass of the molecules.

counterpart. For the present work we have selected Fu et al.'s FF as it is constructed on the basis of a large set of ab initio calculations. Benchmark calculations on benzene and the Zn₄O(HCO₂)₆ cluster model of the α site in MOF-5 show that the overall performance of both FFs are in much closer agreement than one would expect from the inspection of the individual H₂-atomic components (see Figure 6).

It is hard to assess the performance of the different FFs:

ab initio calculations with converged results are difficult for systems that are representable models approximating MOF building blocks. Moreover, the FFs treat H₂ as shapeless particle and thus incorporate implicitly the rotational degrees of freedom. Thus, we will validate the performance of the FF by Fu et al.¹⁰ on the basis of the system that is most-widely studied, MOF-5, also known as IRMOF-1.

VI. HYDROGEN ADSORPTION IN IRMOF-1: THE ROLE OF QUANTUM EFFECTS

Before validating our computational approach, we will first compare the importance of quantum effects on the H_2 adsorption in IRMOF-1. Quantum effects are totally absent in GCMC calculations if the potential resembles the BO potential energy surface, that means, for any potential that has been derived by electronic structure calculations, including the one of Fu et al.,¹⁰ but also those of Han et al.^{44,48} and the COF-FF of Cao et al.⁴³ Therefore, not surprisingly, the classical GCMC isotherm predicts the strongest adsorption capacity (see Figure 7). Inclusion of the semi-classical FH correction, both for the H_2 - H_2 as well as for the H_2 -host potentials, results in a substantial reduction of hydrogen adsorption by $\sim 17\%$ at 77 K for pressures of 20 bar and above. A purely classical LDFT calculation is not possible within our implementation. Even though if the kinetic energy operator is absent in the Hamiltonian, a fair part of this effect is accounted for in the XC potential that refers to the experimental free H_2 isotherm. The significantly lower adsorption of classical LDFT compared to GCMC suggests that quantum effects in the adsorbed H_2 fluid are significant for higher pressures and should not be neglected. This is confirmed by GCMC calculations where the H_2 - H_2 interaction potential is subjected to the semi-classical FH correction (see Figure 7). Indeed, these GCMC results are close to LDFT. Remaining differences are due to many-particle effects in the H_2 fluid and the approximate nature of the FH correction.

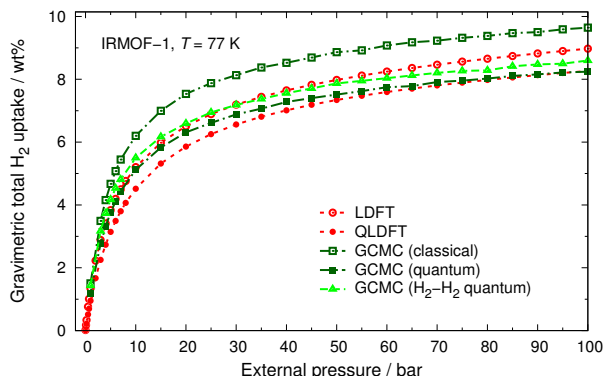


Figure 7. Comparison of gravimetric total adsorption isotherms of IRMOF-1 at $T = 77$ K obtained from classical and quantum calculations using the same interaction potentials and fugacity data.

QLDFT intrinsically accounts for quantum effects by explicit inclusion of the kinetic energy in the Hamiltonian operator. Here, we should note that this inclusion is not exact and follows a simple model, namely by assuming a pseudo one-particle wave function that is obtained as square root of the number density. Physically, this means that all H_2 molecules (bosons) are collapsed in the ground

state. Thus, this approximation works best for low temperatures, and it has indeed been shown that it performs very well for liquid N_2 temperature (77 K).¹⁴ Explicit treatment of quantum effects results again in lowering the H_2 adsorption density. However, the reduction is less compared to the difference between GCMC calculations with and without quantum effects (see Figure 7), due to the fact that quantum effects inside the hydrogen fluid are implicitly considered within classical LDFT. Finally, it should be noted that QLDFT and GCMC calculations with quantum effects differ in the area of moderate pressures, mainly between 10 and 20 bar. As simulation model and interaction potential are identical, and as we can exclude numerical issues for this difference, its origin can either be the presence of many-body effects or the explicit quantum nature of QLDFT, or contributions of both effects.

The QLDFT isotherm for IRMOF-1 is compared with available experimental data from the literature. Our results show that the total gravimetric adsorption isotherm predicted by QLDFT is in excellent agreement with those of Kaye et al.⁴⁹ (after air exposure), Zhou et al.,⁵⁰ and Poirier et al.⁵¹ (see Figure 8). The gravimetric H_2 uptake of IRMOF-1 before air exposure is reported to be higher,⁴⁹ possibly reflecting unsaturated defects in the material. For the calculation of excess isotherms we have subtracted the non-accessible part from the MOF volume. This has been achieved by determining the space where the interaction potential is strongly repulsive (we take the value of 5000 K as cutoff). The resulting QLDFT gravimetric excess isotherm is in close agreement with the experimental data of Zhou et al.⁵⁰ and Poirier et al.,⁵¹ and somewhat higher than the experiments of Kaye et al. (after air exposure)⁴⁹ and of Wong-Foy et al.⁵² We conclude that the QLDFT approach in conjunction with the FF parameters of Fu et al.¹⁰ satisfactorily describes the hydrogen adsorption in this material. In the remainder, we apply this method to the series of IRMOFs, and to MOF-177. These structures incorporate similar building units, thus, we expect them to be well-described by our methodology.

VII. HYDROGEN ADSORPTION IN THE IRMOF SERIES AND MOF-177

After validating our computational approach for IRMOF-1, we apply QLDFT within the same setup as for IRMOF-1 to assess hydrogen adsorption properties at $T = 77$ K on a series of IRMOFs (IRMOF- n with $n = 1, 4, 6, 8, 9, 10, 12, 14, 16, 18$) and MOF-177. In Table I, we list the total gravimetric and volumetric adsorption capacities at 20, 40, 60, 80 and 100 bars, and the excess adsorption at saturation condition. Full isotherms for $P = 0 - 100$ bars are plotted in Figure 9.

Among all the MOFs studied here, at 77 K, IRMOF-16 shows greatest gravimetric hydrogen uptake (17.9 wt% at 100 bar). This structure possesses an extraordinar-

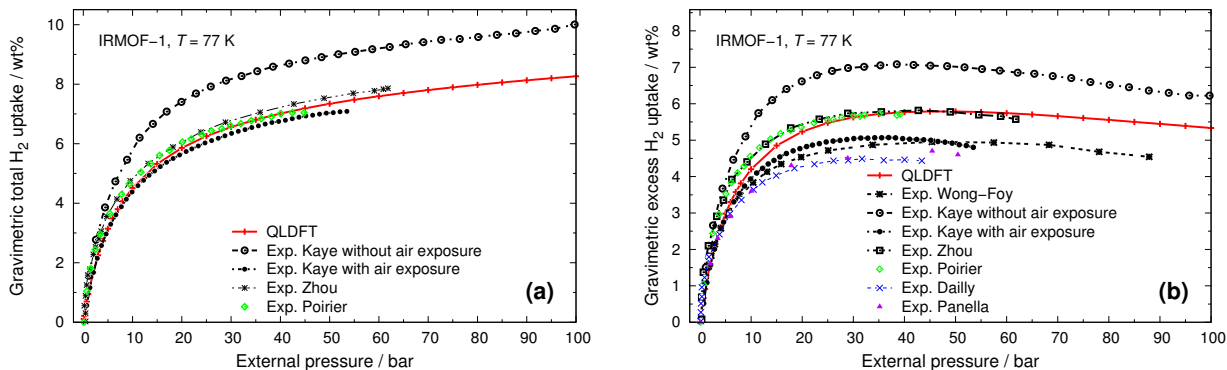


Figure 8. Gravimetric total (a) and excess (b) adsorption isotherms of IRMOF-1 at $T = 77$ K obtained from QLDFT calculations are compared with experiments.^{49–53}

ily large surface area of $6063 \text{ m}^2 \text{ g}^{-1}$, and 84% of its volume is accessible to the H_2 molecules. However, the large free volume, coupled with a low crystal density of 0.21 g cm^{-3} , results in the fact that IRMOF-16 shows the lowest volumetric hydrogen uptake of all MOFs investigated here. A similar trend has been observed for other MOFs, where materials with high gravimetric uptake typically possess low volumetric capacities. Our results show that among the materials considered here the doubly interpenetrated IRMOF-9 framework is the best hydrogen adsorbent on the volumetric basis.

In this study, we did not predict room temperature adsorption capacities. Among others, Frost et al.⁵⁴ already pointed out that the strength of the adsorption potential of these materials is not high enough to adhere sufficient amount of H_2 molecules that fulfil the requirements suggested by the US Department of Energy (DOE) at room temperature.⁵⁵ Fu et al.¹⁰ calculated the room temperature adsorption for the majority of the MOFs studied in this work and confirmed very poor room temperature adsorption. However, our results show that most of the MOFs can even surpass the DOE targets⁵⁵ at technologically plausible liquid N_2 temperature (see Figure 9) at moderate pressures. This may indeed be a viable alternative to high-pressure tanks, as a more flexible tank design would be possible.

In Figure 10, we have plotted the gravimetric total uptakes at 20 bar and excess uptakes at saturation condition against the solvent accessible surface area of corresponding MOFs. Our results show that adsorption capacities at mid pressure regime directly correlate with the solvent accessible surface area and the correlation exists up to the saturation regime (see Figure 10). We have also found a linear correlation between pore volume and gravimetric uptake at 100 bar (see Figure 11). Similar correlations have been reported by Frost et al.²⁷ In order to better illustrate these correlations, we plotted the evolution of adsorbed H_2 density profile inside the IRMOF-1 pore at different pressure loadings (see Figure 12). Due to the attractive host-guest interaction potentials, the first monolayer of adsorbed hydrogen would stay about one molecu-

lar radius apart from the sorbent surface. The formation of few more monolayers is possible, depending on the behavior of how the potential energy diminishes at larger distances. In general, the hydrogen molecules stay close to the surface and rest of the pore remains empty at low pressure. For higher pressures, hydrogen molecules gradually start occupying the pore interior (see Figure 12).

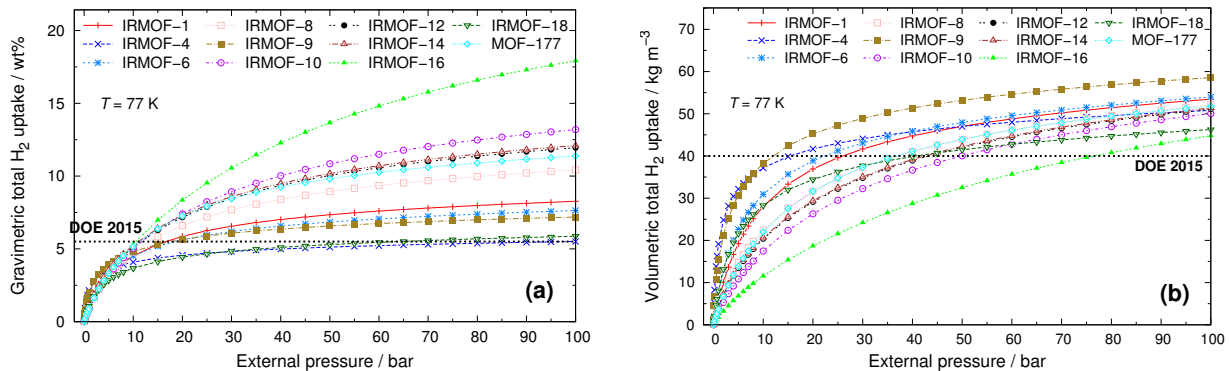
Comparison with experiment and other theoretical studies

To our knowledge, this is the first time that the hydrogen adsorption in a class of MOFs has been investigated using as little empirical tuning as possible. Indeed, to date the hydrogen adsorption properties of the IRMOF series and of MOF-177 have been widely studied by experiments^{31,50–53,56–60} and by computer simulations.^{10,18,27,44,48,61–65} In both cases, it is difficult to arrive at a conclusion on the performance of a particular MOF. On the experimental side, synthesis and transport conditions, defect concentration and experimental details measuring the hydrogen adsorption lead to a rather wide range of observed adsorption capacities. On the other hand, in the majority of the theoretical works, the employed potential models and the computational approaches were calibrated against low pressure (0–1 bar) experimental data. This has led to poor agreement in a wider pressure range.⁶⁶

One should also keep in mind that the conversion of simulation results to the experimental equivalent (i.e., total to excess) or vice versa, required knowledge about the H_2 accessible volume of the frameworks pore and free hydrogen densities at certain thermodynamic condition. This data is another source of uncertainty that can strongly affect the results. Accepting these limitations, a quantitative agreement of adsorption results might be challenging, but a qualitative agreement (curvature of the isotherms) can be achieved.^{10,27,63} Figure 8 exemplifies these facts: our QLDFT determined isotherms of IRMOF-1 match with most of the experiments qualitatively, but quantitative agreement is achieved for few of

Table I. Structural and adsorption properties of MOF systems studied in this work

	Free vol. %	SASA m^2g^{-1}	Total at 20 bar		Total at 40 bar		Total at 60 bar		Total at 80 bar		Total at 100 bar		Excess at saturation		
			wt%	kg m^{-3}	wt%	kg m^{-3}	P/bar	wt%	kg m^{-3}						
IRMOF-1	64.0	3799	5.9	36.9	7.0	44.7	7.6	48.8	8.0	51.4	8.3	53.5	45	5.8	36.5
IRMOF-4	39.6	2170	4.6	41.7	5.0	45.7	5.2	48.0	5.4	49.6	5.5	50.8	45	4.4	40.5
IRMOF-6	58.8	3467	5.6	38.9	6.6	45.9	7.1	49.6	7.4	52.1	7.6	54.0	45	5.5	38.3
IRMOF-8	70.7	4436	6.6	31.6	8.4	41.1	9.4	46.2	10.0	49.6	10.4	52.1	55	6.7	32.3
IRMOF-9	55.8	3746	5.6	45.2	6.4	51.4	6.7	54.6	7.0	56.9	7.2	58.6	45	5.5	44.1
IRMOF-10	77.4	4923	7.4	26.3	10.0	36.6	11.5	42.8	12.5	46.9	13.2	50.0	60	7.7	27.5
IRMOF-12	74.3	4939	7.2	29.1	9.4	38.9	10.6	44.5	11.4	48.3	12.0	51.1	55	7.4	29.9
IRMOF-14	75.0	4783	7.3	29.4	9.5	39.2	10.7	44.8	11.5	48.6	12.1	51.4	55	7.4	30.0
IRMOF-16	84.1	6063	8.3	18.7	12.3	28.7	14.8	35.7	16.6	40.8	17.9	44.8	70	8.6	19.2
IRMOF-18	48.2	2571	4.4	34.4	5.1	39.9	5.5	42.8	5.7	44.7	5.9	46.2	45	4.3	33.6
MOF-177	70.3	4901	7.3	31.6	9.2	41.1	10.3	46.1	10.9	49.4	11.4	51.8	55	7.4	32.3

Figure 9. Predicted gravimetric (a) and volumetric (b) total H_2 adsorption isotherms of MOFs at $T = 77$ K.

them only.

In Table II, we have compared the adsorption capacities of the MOF systems determined from our QLDFT calculations with available experimental and simulation data. Except for IRMOF-8, our predicted results are in good agreement with literature data. In the worst case, IRMOF-8, our excess isotherms significantly exceed the experimental results of Panella et al.⁵⁹ and Dailly et al.,⁵⁷ who have reported that IRMOF-8 gets saturated at the 10–15 bar pressure range adsorbing 3.6 wt% H_2 , while our calculations indicate that IRMOF-8 can adsorb a maximum 6.7 wt% at 55 bar. Independently, Garberoglio et al.⁶⁴ also predicted a saturation pressure similar to ours, even with higher adsorption (~ 8.3 wt%). GCMC simulations of Fu et al.,¹⁰ Frost et al.,²⁷ and Yang and Zhong¹⁸ also predicted higher adsorption compared to experiments. In addition, we have thoroughly compared our QLDFT results with Fu et al.’s¹⁰ Feynman-Hibbs quantum corrected and Frost et al.’s²⁷ classical GCMC results for the same MOF systems studied in this work. In terms of gravimetric total uptakes at 80 bar, Fu et al.’s and Frost et al.’s consistently predict higher hydrogen uptake by 5–10% and 12–19%, respectively.

VIII. CONCLUSION

We have calculated the role of quantum effects on the adsorption of molecular hydrogen in metal-organic frame-

works. The inclusion of quantum effects significantly reduces the hydrogen adsorption capacity at liquid N_2 temperature ($T = 77$ K) compared to classical simulations, and therefore it is crucial to include them in the calculation in order to make correct predictions. They can be included either explicitly, e.g. within Quantized Liquid Density-Functional Theory, or semi-classically in any classical method of statistical mechanics as for example the Grand Canonical Monte-Carlo approach. Both approaches are computationally competitive, QLDFT having the advantage that it implicitly accounts for many-body effects via the XC potential, while GCMC is suitable to treat hydrogen as diatomic species beyond the shapeless particle approximation. It remains challenging to have a satisfactorily working host-guest potential, first as two-body force fields are intrinsically limited in their accuracy, and as high-quality reference calculations are computationally demanding.

Our calculations are, however, in good agreement with experimental data. At technologically applicable liquid N_2 temperature ($T = 77$ K) and moderate pressure (20 bar or even less), many MOFs fulfil the requirements of the US Department of Energy of 5.5 wt% gravimetric and 40 kg m^{-3} volumetric storage capacity, which however are defined for room temperature storage. It should be noted, though, that the choice for the best MOF material depends on the technological context: Those frameworks with exceptionally high gravimetric storage capacity perform poorly in volumetric storage and vice versa. Results

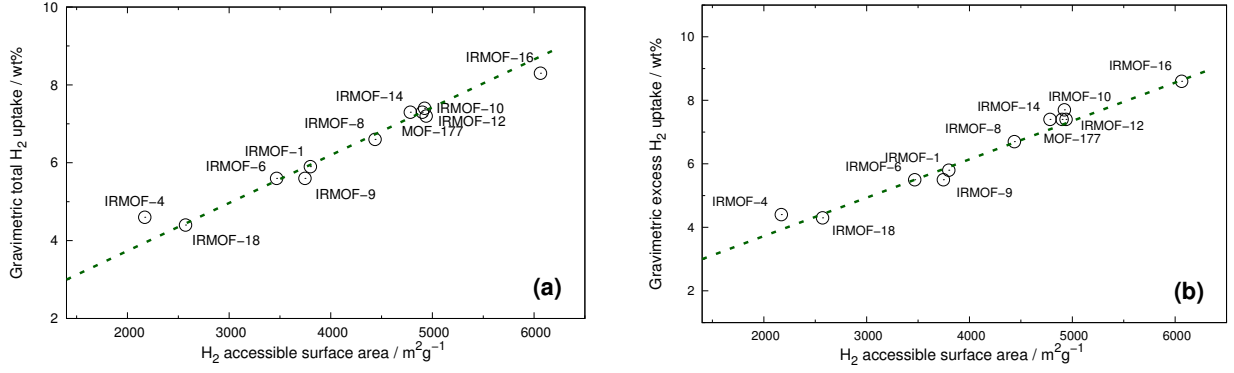


Figure 10. Relationship between H_2 accessible surface area and gravimetric total H_2 adsorption at $P = 20$ bar (a), and gravimetric excess H_2 adsorption at saturation pressures (b).

Table II. QLDFT determined H_2 adsorption results are compared with experiments and GCMC data^a

	Excess uptake at 77 K		Total uptake at 77 K		Method and Ref.
	P / bar	wt%	P / bar	wt%	
IRMOF-1	30*	4.3			Exp. [57]
	45*	4.7			Exp. [53]
	45*	4.9			Exp. [52]
	40*	5.1 ^b , 7.1 ^c	45	6.9 ^b , 8.8 ^c	Exp. [49]
	45*	5.8	45	7.4	Exp. [50]
	45*	5.8	45	7.2	QLDFT
IRMOF-4			80	5.1	GCMC [27]
			80	5.4	QLDFT
IRMOF-6	45*	4.6			Exp. [52]
	45*	5.5	80	7.4	QLDFT
			80	8.3	GCMC [27]
IRMOF-8	10–15*	3.6			Exp. [57,59]
	10–15	4.3–5.1			QLDFT
	55*	6.7	80	10.0	QLDFT
	50*	8.3	80	11.9	GCMC [64]
	80	7.7	80	10.8	GCMC [10]
			80	11.8	GCMC [27]
IRMOF-9	1	1.2			Exp. [56]
	1	1.9	80	7.0	QLDFT
			80	7.7	GCMC [10]
IRMOF-10			80	13.4	GCMC [10]
			80	14.7	GCMC [27]
			80	12.5	QLDFT
IRMOF-12			80	13.4	GCMC [27]
			80	11.4	QLDFT
IRMOF-14	50*	10	100	14.6	GCMC [64]
	55*	7.4	100	12.1	QLDFT
IRMOF-16			80	18.0	GCMC [10]
			80	19.7	GCMC [27]
			80	16.6	QLDFT
IRMOF-18	1	0.9			Exp. [31]
	1	1.0	80	5.7	QLDFT
			80	5.5	GCMC [27]
MOF-177	52–66*	6.8–7.1	72–75	10.0–10.3	Exp. [58]
	69*	7.0	78	10.2	Exp. [52]
	55*	7.4	75	10.0	QLDFT

^a: some data points are extracted from the published figures, consider a small deviation from the original.

^b and ^c: sample prepared with and without air exposure

* indicates the pressure at which the system reached its maximum excess adsorption

also depend on the target pressure that is suitable in the system. Thus, the implementation of a H_2 storage facilities using MOFs are technologically possible, though economically demanding.

Finally, we conclude that our QLDFT approach is an available and computationally feasible alternative to popular classical or semi-classical approaches of statistical

mechanics that allows the explicit treatment of quantum effects and implicitly includes many-body interactions in the adsorbed hydrogen fluid.

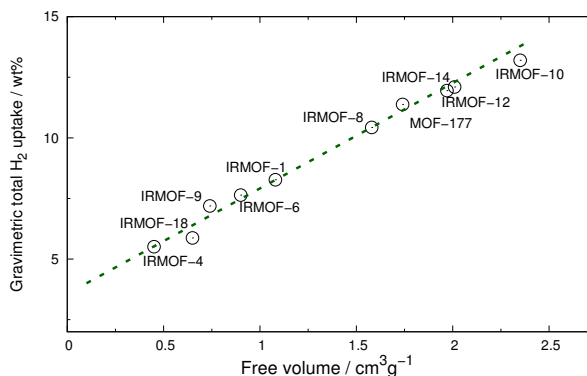


Figure 11. Relationship between H_2 accessible free volume and total amount of adsorbed H_2 at $P = 100$ bar.

ACKNOWLEDGMENTS

This work has been supported by the European Research Council (ERC-StG, GA 256962) and Deutsche Forschungsgemeinschaft (GA HE 3543/7-2). We thank Dr. A. Martínez-Mesa for providing the subroutine of Leachman et al.'s EOS.

REFERENCES

- ¹M. P. Suh, H. J. Park, T. K. Prasad, and D.-W. Lim, *Chem. Rev.* **112**, 782 (2012).
- ²H. Oh, I. Savchenko, A. Mavrandonakis, T. Heine, and M. Hirscher, *ACS Nano* **8**, 761 (2014).
- ³M. Hirscher, ed., *Handbook of Hydrogen Storage* (Wiley-VCH Verlag GmbH & Co. KGaA, Weinheim, Germany, 2010).
- ⁴M. Eddaoudi, J. Kim, N. Rosi, D. Vodak, J. Wachter, M. O’Keeffe, and O. M. Yaghi, *Science* **295**, 469 (2002).
- ⁵H. K. Chae, D. Y. Siberio-Pérez, J. Kim, Y. Go, M. Eddaoudi, A. J. Matzger, M. O’Keeffe, and O. M. Yaghi, *Nature* **427**, 523 (2004).
- ⁶H. Furukawa, N. Ko, Y. B. Go, N. Aratani, S. B. Choi, E. Choi, A. O. Yazaydin, R. Q. Snurr, M. O’Keeffe, J. Kim, and O. M. Yaghi, *Science* **329**, 424 (2010).
- ⁷O. K. Farha, A. O. Yazaydin, I. Eryazici, C. D. Malliakas, B. G. Hauser, M. G. Kanatzidis, S. T. Nguyen, R. Q. Snurr, and J. T. Hupp, *Nat. Chem.* **2**, 944 (2010).
- ⁸S. S. Han, J. L. Mendoza-Cortés, and W. A. Goddard, *Chem. Soc. Rev.* **38**, 1460 (2009).
- ⁹R. B. Getman, Y.-S. Bae, C. E. Wilmer, and R. Q. Snurr, *Chem. Rev.* **112**, 703 (2012).
- ¹⁰J. Fu and H. Sun, *J. Phys. Chem. C* **113**, 21815 (2009).
- ¹¹R. P. Feynman and A. R. Hibbs, *Quantum Mechanics and Path Integrals* (McGraw-Hill, New York, 1965).
- ¹²S. Patchkovskii and T. Heine, *Phys. Rev. E* **80**, 031603 (2009).
- ¹³A. Martínez-Mesa, L. Zhechkov, S. N. Yurchenko, T. Heine, G. Seifert, and J. Rubayo-Soneira, *J. Phys. Chem. C* **116**, 19543 (2012).
- ¹⁴C. F. J. Walther, S. Patchkovskii, and T. Heine, *J. Chem. Phys.* **139**, 034110 (2013).
- ¹⁵D. Frenkel and B. Smit, *Understanding Molecular Simulation: From Algorithms to Applications* (Academic Press, San Diego, 2002).
- ¹⁶W. Saam and C. Ebner, *Phys. Rev. A* **15**, 2566 (1977).
- ¹⁷Q. Wang, J. K. Johnson, and J. Q. Broughton, *J. Chem. Phys.* **107**, 5108 (1997).
- ¹⁸Q. Yang and C. Zhong, *J. Phys. Chem. B* **109**, 11862 (2005).
- ¹⁹A. Martínez-Mesa, S. N. Yurchenko, S. Patchkovskii, T. Heine, and G. Seifert, *J. Chem. Phys.* **135**, 214701 (2011).
- ²⁰S. Patchkovskii and T. Heine, *Phys. Chem. Chem. Phys.* **9**, 2697 (2007).
- ²¹B. Lukose, M. Wahiduzzaman, A. Kuc, and T. Heine, *J. Phys. Chem. C* **116**, 22878 (2012).
- ²²J. Teufel, H. Oh, M. Hirscher, M. Wahiduzzaman, L. Zhechkov, A. Kuc, T. Heine, D. Denysenko, and D. Volkmer, *Adv. Mater.* **25**, 635 (2013).
- ²³R. Car and M. Parrinello, *Phys. Rev. Lett.* **55**, 2471 (1985).
- ²⁴A. Gupta, S. Chempath, M. J. Sanborn, L. A. Clark, and R. Q. Snurr, *Mol. Simul.* **29**, 29 (2003).
- ²⁵J. W. Leachman, R. T. Jacobsen, S. G. Penoncello, and E. W. Lemmon, *J. Phys. Chem. Ref. Data* **38**, 721 (2009).
- ²⁶T. Duren, F. Millange, G. Ferey, K. Walton, and R. Snurr, *J. Phys. Chem. C* **111**, 15350 (2007).
- ²⁷H. Frost, T. Düren, and R. Q. Snurr, *J. Phys. Chem. B* **110**, 9565 (2006).
- ²⁸V. Buch, *J. Chem. Phys.* **100**, 7610 (1994).
- ²⁹W. Humphrey, A. Dalke, and K. Schulten, *J. Mol. Graph.* **14**, 33 (1996).
- ³⁰A. Varshney, F. Brooks, and W. Wright, *IEEE Comput. Graph. Appl.* **14**, 19 (1994).
- ³¹J. L. C. Rowsell, A. R. Millward, K. S. Park, and O. M. Yaghi, *J. Am. Chem. Soc.* **126**, 5666 (2004).
- ³²A. Kuc, A. Enyashin, and G. Seifert, *J. Phys. Chem. B* **111**, 8179 (2007).
- ³³B. Lukose, B. Supronowicz, P. St. Petkov, J. Frenzel, A. B. Kuc, G. Seifert, G. N. Vayssilov, and T. Heine, *Phys. status solidi* **249**, 335 (2012).
- ³⁴R. D. Goodwin, D. E. Diller, H. M. Roder, and L. A. Weber, *J. Res. Natl. Bur. Stand. Sect. A Phys. Chem.* **67A**, 173 (1963).
- ³⁵“NIST Standard Reference Database 69: NIST Chemistry WebBook,” <http://webbook.nist.gov>, Accessed on March 1, 2014.
- ³⁶van der Waals Johannes Diderik, *On the Continuity of the Gaseous and Liquid States*, Ph.D. thesis, Universiteit Leiden (1873).
- ³⁷D.-Y. Peng and D. B. Robinson, *Ind. Eng. Chem. Fundam.* **15**, 59 (1976).
- ³⁸R. L. Mills, D. H. Liebenberg, J. C. Bronson, and L. C. Schmidt, *J. Chem. Phys.* **66**, 3076 (1977).
- ³⁹P. Diep and J. K. Johnson, *J. Chem. Phys.* **112**, 4465 (2000).
- ⁴⁰A. Michels, W. de Graaff, and C. Ten Seldam, *Physica* **26**, 393 (1960).
- ⁴¹S. L. Mayo, B. D. Olafson, and W. A. Goddard, *J. Phys. Chem.* **94**, 8897 (1990).
- ⁴²a. K. Rappe, C. J. Casewit, K. S. Colwell, W. a. Goddard, and W. M. Skiff, *J. Am. Chem. Soc.* **114**, 10024 (1992).
- ⁴³D. Cao, J. Lan, W. Wang, and B. Smit, *Angew. Chem. Int. Ed. Engl.* **48**, 4730 (2009).
- ⁴⁴S. S. Han, W.-Q. Deng, and W. A. Goddard, *Angew. Chem. Int. Ed. Engl.* **46**, 6289 (2007).
- ⁴⁵T. Heine, L. Zhechkov, and G. Seifert, *Phys. Chem. Chem. Phys.* **6**, 980 (2004).
- ⁴⁶S. Patchkovskii, J. S. Tse, S. N. Yurchenko, L. Zhechkov, T. Heine, and G. Seifert, *Proc. Natl. Acad. Sci. U. S. A.* **102**, 10439 (2005).
- ⁴⁷A. Kuc, T. Heine, G. Seifert, and H. a. Duarte, *Theor. Chem. Acc.* **120**, 543 (2008).
- ⁴⁸S. S. Han and W. A. Goddard, *J. Phys. Chem. C* **112**, 13431 (2008).
- ⁴⁹S. S. Kaye, A. Dailly, O. M. Yaghi, and J. R. Long, *J. Am. Chem. Soc.* **129**, 14176 (2007).
- ⁵⁰W. Zhou, H. Wu, M. Hartman, and T. Yildirim, *J. Phys. Chem. C* **111**, 16131 (2007).
- ⁵¹E. Poirier and A. Dailly, *J. Phys. Chem. C* **112**, 13047 (2008).
- ⁵²A. G. Wong-Foy, A. J. Matzger, and O. M. Yaghi, *J. Am. Chem.*

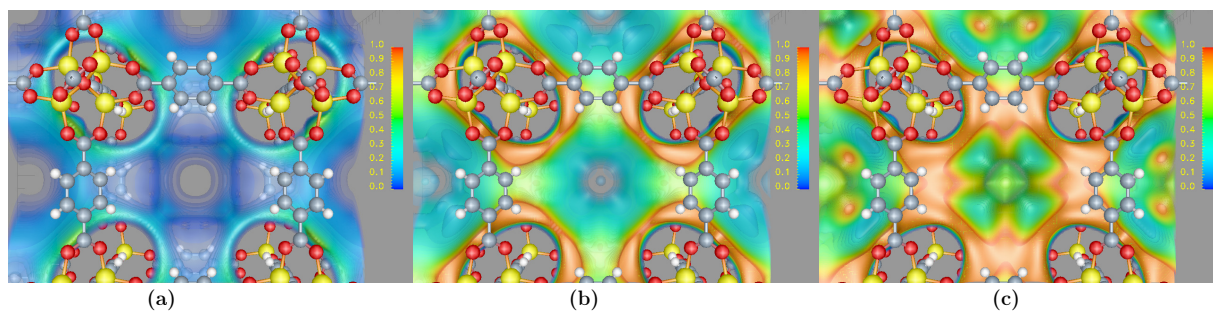


Figure 12. Normalized density profiles of adsorbed H_2 inside the unit cell of IRMOF-1 at $T = 77$ K, and $P = 1$ bar (a), 10 bar (b) and 100 bar (c).

- Soc. **128**, 3494 (2006).
- ⁵³B. Panella, M. Hirscher, H. Pütter, and U. Müller, *Adv. Funct. Mater.* **16**, 520 (2006).
- ⁵⁴H. Frost and R. Q. Snurr, *J. Phys. Chem. C* **111**, 18794 (2007).
- ⁵⁵“U.S. DOE; Targets for Onboard Hydrogen Storage Systems for Light-Duty Vehicles,” http://energy.gov/sites/prod/files/2014/03/f11/targets_onboard_hydro_storage_explanation.pdf, Accessed on June 4, 2014.
- ⁵⁶J. L. C. Rowsell and O. M. Yaghi, *J. Am. Chem. Soc.* **128**, 1304 (2006).
- ⁵⁷A. Dailly, J. J. Vajo, and C. C. Ahn, *J. Phys. Chem. B* **110**, 1099 (2006).
- ⁵⁸H. Furukawa, M. A. Miller, and O. M. Yaghi, *J. Mater. Chem.* **17**, 3197 (2007).
- ⁵⁹B. Panella, K. Hönes, U. Müller, N. Trukhan, M. Schubert, H. Pütter, and M. Hirscher, *Angew. Chem. Int. Ed. Engl.* **47**, 2138 (2008).
- ⁶⁰M. Hirscher, B. Panella, and B. Schmitz, *Microporous Mesoporous Mater.* **129**, 335 (2010).
- ⁶¹D. H. Jung, D. Kim, T. B. Lee, S. B. Choi, J. H. Yoon, J. Kim, K. Choi, and S.-H. Choi, *J. Phys. Chem. B* **110**, 22987 (2006).
- ⁶²S. S. Han and G. William A, *J. Am. Chem. Soc.* **129**, 8422 (2007).
- ⁶³P. Ryan, L. J. Broadbelt, and R. Q. Snurr, *Chem. Commun. (Camb)*, 4132 (2008).
- ⁶⁴G. Garberoglio, A. I. Skoulidas, and J. K. Johnson, *J. Phys. Chem. B* **109**, 13094 (2005).
- ⁶⁵E. Klontzas, A. Mavrandonakis, E. Tylianakis, and G. E. Froudakis, *Nano Lett.* **8**, 1572 (2008).
- ⁶⁶S. Keskin, J. Liu, R. B. Rankin, J. K. Johnson, and D. S. Sholl, *Ind. Eng. Chem. Res.* **48**, 2355 (2009).